MIT Libraries | DSpace@MIT

MIT Open Access Articles

Investigation of a Multiple Impeller Design
for a High Performance Air-Cooled Heat Sink

Citation: Staats, Wayne L., et al. "Investigation of a Multiple Impeller Design for a High Performance Air-Cooled Heat Sink." Proceedings of the ASME 2010 International Mechanical Engineering Congress & Exposition, 12-18 November, 2010, Vancouver, British Columbia, Canada, ASME, 2010, pp. 313–20. © 2010 ASME

As Published: http://dx.doi.org/10.1115/IMECE2010-40703

Publisher: ASME International

Persistent URL: http://hdl.handle.net/1721.1/119157

Version: Final published version: final published article, as it appeared in a journal, conference proceedings, or other formally published context

Massachusetts Institute of Technology

IMECE2010-40703

INVESTIGATION OF A MULTIPLE IMPELLER DESIGN FOR A HIGH PERFORMANCE AIR-COOLED HEAT SINK

Wayne L. Staats
wstaats@mit.edu

Teresa B. Peters
teresab@mit.edu

Jon M. Allison
allj@mit.edu

Matthew McCarthy
mattmcc@mit.edu

Evelyn N. Wang
enwang@mit.edu

John G. Brisson
brisson@mit.edu

Massachusetts Institute of Technology, Department of Mechanical Engineering
77 Massachusetts Avenue, Cambridge, Massachusetts 02139 U.S.A.

ABSTRACT

A high-performance air-cooled heat sink that incorporates a novel heat pipe with multiple parallel condenser layers and interdigitated blower impellers is presented. A flow circuit model was developed in order to predict the air flow performance of a 15-layer impeller system using experimental measurements from a single layer. A 15-layer impeller system was constructed to validate the flow circuit model. The performance of the multi-layer system was investigated by using a hot wire anemometer to compare flow between layers and by measuring the inflation rate of a bag enclosing the air outlets. This work addresses important issues that allow the extension of the air flow modeling and experimental results from a single impeller design to a multilayer stack of impellers operating in parallel and sharing a common inlet.

Keywords: heat pipe; heat exchanger; multilayer blower; flow circuit; hydraulic circuit.

INTRODUCTION

With the advancement of high performance electronics, the large heat generation rates are demanding creative new thermal solutions. A compact air-cooled loop heat pipe is being developed to provide efficient cooling to electronics and minimize the electrical power input required. An exploded view of the device can be seen in Fig. 1. The device has a footprint of 101.6 x 101.6 mm and is 101.6 mm tall. Heat enters the device via the evaporator on the bottom, where water vapor is generated and flows up through two vertical fluid connectors into a multitude of flat, air-cooled condensers. Heat is transferred to the air through the walls of the condensers as the water vapor condenses. A sintered wicking structure returns the condensate to the evaporator via the remaining two fluid connectors.
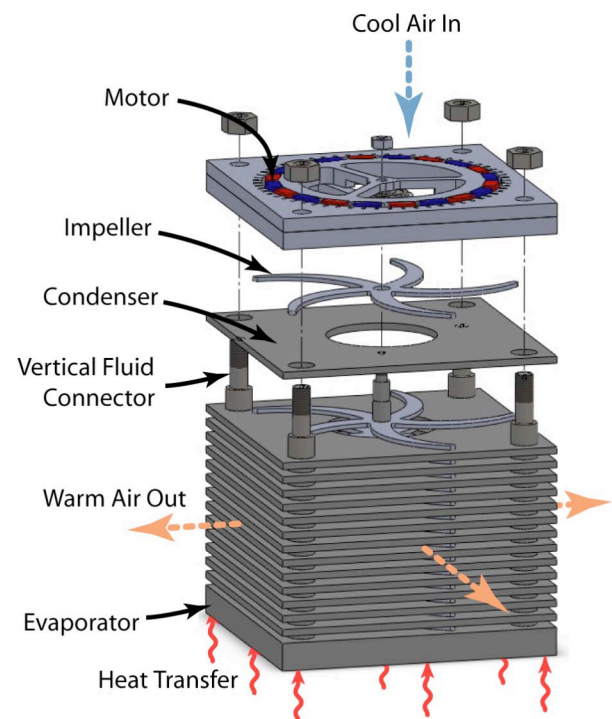

Figure 1. An exploded view of the 15-layer device.

Multiple layers are necessary for condensation because the thermal resistance to the air flow from the condensers is the dominant resistance in the system. Air is drawn through the opening in the top and exhausted out the four sides by impellers located between the condenser plates and driven by a common shaft. A low-profile permanent magnet synchronous motor, which is integral to the top plate, drives the impeller shaft. This arrangement gives a high heat transfer conductance to the air

from the condensers with a relatively small power input to the motor, allowing the device to provide cooling with a high coefficient of performance.

Heat exchangers cooled by forced air convection have undergone significant development and optimization particularly for electronic equipment packaging [1]. Enhancement of air-cooled devices for high-power equipment involves an integrated approach including materials, fin geometries and air flow performance [2]. There are several examples of recent work directed to optimization of fin geometry for heat transfer, fluid friction and entropy generation with airflow supplied by an external fan, for example [3, 4]. Integrating the forced convection pumping components and the heat transfer surfaces enables compact air-cooled heat transfer devices. For example, Walsh et al. [5] and Stafford et al. [6] investigated integration of low-profile radial fans with finned and finless heat sinks and found that heat transfer could be improved significantly by varying the fin-airflow geometry without major changes in pumping power. In contrast to these finned, air-cooled heat exchangers, the multiple-impeller device discussed here uses impeller blades adjacent and parallel to the heat transfer surfaces.

In this work, the performance of the blower for this heat sink design is discussed and characterized. Initial tests were performed on a single layer apparatus that consisted of a single impeller rotating between two parallel plates. Similar measurements of a 15-layer device showed that a simple scaling of the single layer results over-predicted the flows measured in the 15-layer device. To explain the disparity a simple circuit model was developed that reconciles these two measurements and allows the prediction of multilayer heat exchanger flow performance with single layer flow measurements. In what follows, the single layer measurements and results are presented. A flow circuit model is developed, and its results are compared to experimental results on a multilayer device with a similar flow configuration as that shown in Fig. 1.

SINGLE LAYER CHARACTERIZATION

A single layer apparatus (Figs. 2 and 3) was constructed to characterize the performance of a single impeller. A Delrin top plate is separated from a copper bottom plate by precision shims at each corner. Air enters the layer through a 40 mm inner diameter "chimney" extending upwards from the top plate. The chimney contains a flow-straightening screen near the top and a pressure tap near the bottom. The pressure difference between the chimney and ambient was measured by a differential pressure sensor (DC002NDC4, Honeywell). The flow rate was measured with a rotameter (FP1-35-G-10 tube with 1-GUSVT-611 float, Fischer & Porter Co.) upstream of the chimney; the temperature of the air entering the rotameter was measured with a silicon diode temperature sensor (DT-470-SD, Lakeshore).

A DC motor (110930, Maxon) was used to drive the shaft and impeller. The rotational speed of the shaft was measured

with an incremental encoder (EM-1-32 encoder with HUBDISK-2-64-472-I codewheel, US Digital). A two-axis micrometer translation stage allowed the shaft to be accurately centered with respect to the plate and a two-axis tilt stage provided adjustment to ensure that the impeller rotated in a plane parallel to the stationary plates. Another micrometer stage allowed the height of the impeller to be finely adjusted.
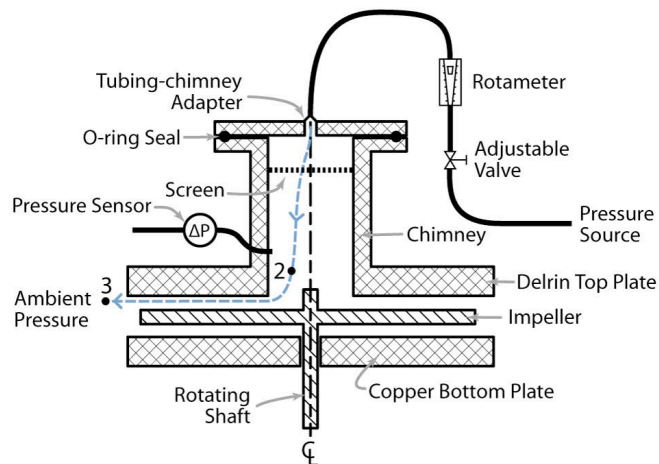

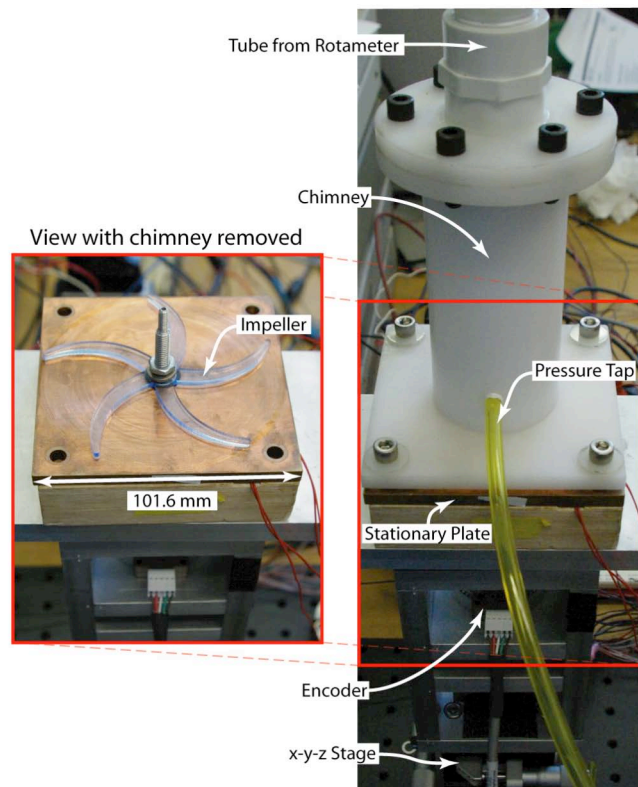**Figure 2. A schematic of the single layer test apparatus.**

Figure 3. An apparatus to characterize a single impeller layer.

Copyright © 2010 by ASME

The pump performance measurements for a chosen stator and impeller geometry were performed by first rotating the impeller at fixed speed. An adjustable valve upstream of the rotameter provided a flow resistance between a source of pressurized air and the low pressure region just upstream of the impeller gap (point 2 in Fig. 2). Next, the maximum pressure rise of the blower (ΔP_{max}) was measured by completely closing the valve and recording the pressure difference between the chimney and ambient. Subsequent operating points were obtained by incrementally opening the valve and measuring the differential pressure and the flow rate through the rotameter. The temperature near the rotameter was also recorded to correct for variations in the air temperature (density) entering the system.

A pump curve was obtained for a single layer impeller rotating at a fixed speed. The impeller, shown to scale in Fig. 4, has five swept-back blades, a thickness of 1.5 mm and fits in a 101 mm diameter circle. The impeller operated in a 2.8 mm tall channel. The geometry tested is representative of an optimized single layer design, a thorough discussion of which can be seen in Allison [7]. At each operating point in the test, 1000 pressure measurements were taken over the course of several seconds and averaged; the uncertainty was estimated by the standard deviation of these measurements. A density correction was applied to the indicated rotameter flow rate since the calibration curve for the rotameter was generated under slightly different conditions than in the experiments. The rotameter uncertainty was estimated to be about 2 percent of its full scale value of 3.3 L/s, based on literature from the manufacturer.

The pressure rise of the single blower, plotted as a function of the volume flow and with a linear fit, can be seen in Fig. 5. The linear fit provides a satisfactory approximation to the data; this has implications that are discussed below.
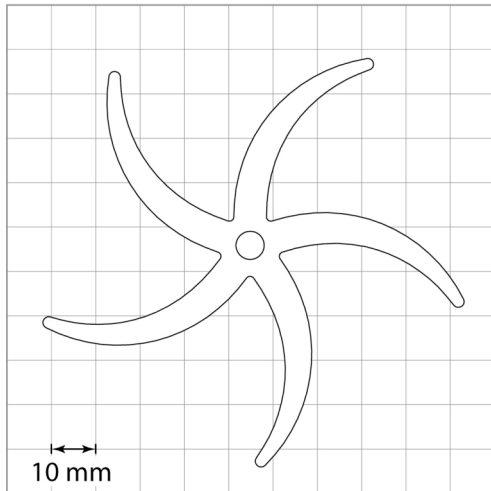

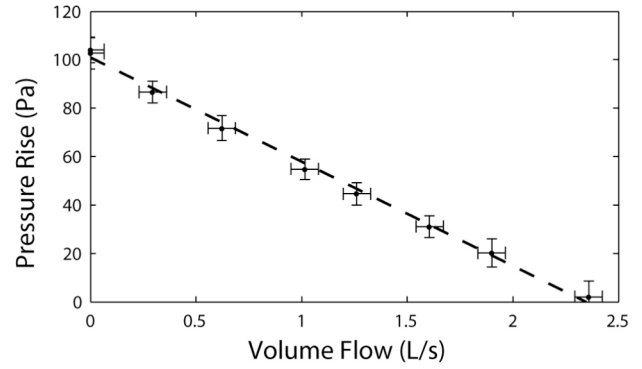**Figure 4. A top view of the impeller characterized in the single layer test.**

Figure 5. An experimentally determined pump curve for the impeller shown in Fig. 4 operating at 4400 rpm. A best-fit line is superimposed to show the linearity of the data.

FLOW CIRCUIT MODEL

A flow circuit model was developed to better understand the flow drivers and resistors. First, a system with a single layer was analyzed using the model shown in Fig. 6. Air flow enters the device inlet from an infinite, stagnant reservoir at ambient pressure (point 1). The flow is accelerated from the stagnation state to some velocity at point 2 as it enters the device. The flow from point 1 to point 2 experiences a minor loss associated with the flow contraction. Next, the impeller pumps the flow from point 2 to point 3, where it discharges to ambient pressure.
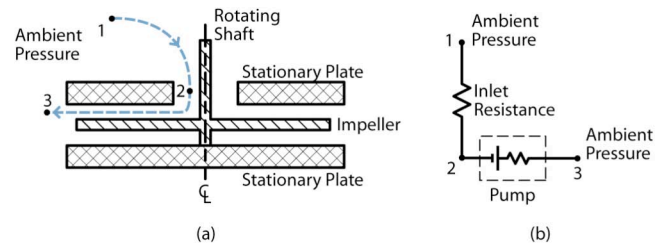

Figure 6. (a) A cross sectional view of the single layer model. (b) A flow circuit representation of the single layer model.

The flow along streamline 1-2 is characterized by the energy equation with a minor loss term due to the entrance effects:

$$\frac{P_1}{\rho} - \left(\frac{P_2}{\rho} + \frac{v_2^2}{2} \right) = K \frac{v_2^2}{2} \qquad (1)$$

where P is the pressure, ρ is the density, v is the velocity, and K is a coefficient associated with the minor losses in the flow from point 1 to point 2. The velocity at point 1 is zero since the device draws air from a stagnant reservoir.

3

Copyright © 2010 by ASME

Furthermore, the volume flow rate through the device, $\dot{V}$, is

$$\dot{V} = A_2 v_2 \qquad (2)$$

where A_2 is the cross sectional area at point 2. Substituting Eq. (2) into Eq. (1) and rearranging yields

$$P_1 - P_2 = \frac{\rho(K+1)\dot{V}}{2A_2^2}\dot{V} \qquad (3)$$

Equation (3) shows a relationship between the pressure difference between points 1 and 2 and the volume flow rate. By comparison, the flow of electric current through a resistor is given by Ohm's law:

$$\Delta V = R_{\text{elec}} I \qquad (4)$$

where ΔV is the voltage drop across the resistor, R_{elec} is the electrical resistance and I is the current through the resistor.

Equations (3) and (4) are similar in that they describe the relationship between a driving potential and a flow. Equation (3) can be cast into the form of Eq. (4) by recognizing that ΔV in Eq. (4) corresponds to $P_1 - P_2$ in Eq. (3), that I corresponds to $\dot{V}$, and R_{elec} corresponds to R_{inlet} where

$$R_{\text{inlet}} = \frac{\rho(K+1)\dot{V}}{2A_2^2} \qquad (5)$$

The inlet resistance in this case is not constant since it depends on the volume flow rate $\dot{V}$.

The flow in the pump section between points 2 and 3 is modeled using the pump curve. It has already been shown that the pressure rise across the pump is a linearly decreasing function of the volume flow rate. Mathematically, this means the pressure increase across the pump ($P_3 - P_2$) is linearly related to the volume flow rate as

$$P_3 - P_2 = \Delta P_{\text{max}} - R_{\text{int}} \dot{V}_{\text{layer}} \qquad (6)$$

where ΔP_{max} is the zero flow pressure rise of the pump and $-R_{\text{int}}$ is the slope of the pump curve. Figure 7 shows a representation of the pump curve and the corresponding equivalent circuit (the Thévenin equivalent). The values for ΔP_{max} and R_{int} that correspond to the measured pump curve in Fig. 5 are 101 Pa and 43×10^3 Pa·s/m³, respectively.
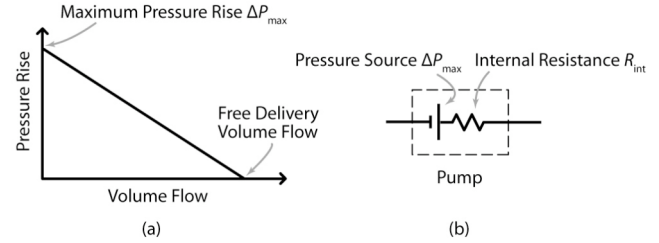

Figure 7. (a) A linearized pump curve, similar to that shown in Fig. 5. (b) A Thévenin equivalent circuit representing the pump whose curve is shown in (a). The equivalent circuit consists of an ideal pressure source and a constant internal flow resistance.

With the linearized pump curve, the single layer flow circuit has been reduced to two elements: the pump, represented by an ideal voltage source, ΔP_{max}, and internal resistance, R_{int}, and the inlet, represented by a single nonlinear resistor, R_{inlet}. This model can be extended to represent a multilayer device like that shown in Fig. 8. The impeller layers in the multilayer device are geometrically identical to the single layer characterized above, and hence the linear pump curve representation developed for the single layer model may be incorporated into the multilayer model. Since the hydraulic diameter of each layer is small in comparison to the inlet diameter, the area in the center of the device acts like a plenum and the resistance between the layers can be neglected. In fact, anemometer tests discussed below confirmed that, for a given operating point, the flow in each layer is approximately the same. This observation proves that the interlayer flow resistance is negligible. The flow circuit for an n-layer device is then represented by an inlet resistance followed by multiple pumps acting in parallel as shown in Fig. 8b.
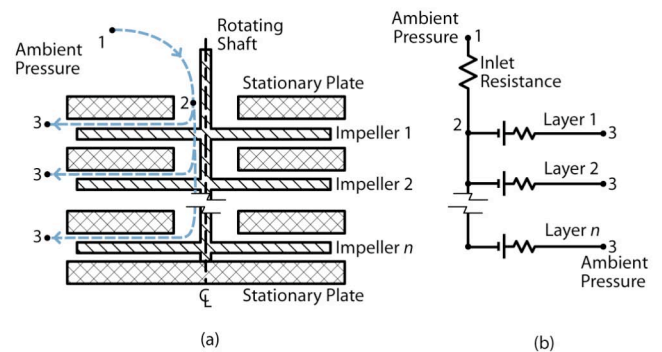

Figure 8. (a) A cross sectional view of the n-layer model. (b) A flow circuit representation of the n-layer model.

The resistor network can be analyzed using loop equations [8], recognizing that the pressure (potential) for point 1 and all points 3 is the same. The loop equations are:

$$\text{Layer 1:} \qquad \Delta P_{\text{max}} = \dot{V} R_{\text{inlet}} + \dot{V}_1 R_{\text{int}}$$

4   Copyright © 2010 by ASME

Layer 2: $\quad \Delta P_{max} = \dot{V}R_{inlet} + \dot{V}_2 R_{int}$

$$\vdots$$

Layer n: $\quad \Delta P_{max} = \dot{V}R_{inlet} + \dot{V}_n R_{int}$ (7)

where $\dot{V}_1$, $\dot{V}_2$, and $\dot{V}_n$ are the volume flow rates through layers 1, 2, and n, respectively. $\dot{V}$ is, once again, the total volume flow rate through the inlet resistance. Continuity requires that

$$\dot{V} = \sum_{j=1}^{n} \dot{V}_j \quad (8)$$

Equations (7) can be summed and using Eq. (8), ΔP_{max} can be related to the total volume flow $\dot{V}$ as

$$\Delta P_{max} = \left(R_{inlet} + \frac{R_{int}}{n} \right)\dot{V} = \left(\frac{\rho(K+1)\dot{V}}{2A_2^2} + \frac{R_{int}}{n} \right)\dot{V} \quad (9)$$

This equation can be explicitly solved for the volume flow rate through the stack as a function of the number of layers in the stack as

$$\dot{V} = \frac{R_{int}}{n} \frac{A_2^2}{\rho(K+1)}\left(\sqrt{1 + \frac{2\rho(K+1)}{A_2^2}\frac{n^2}{R_{int}^2}\Delta P_{max}} - 1 \right) \quad (10)$$

Figure 9 shows the calculated volume flow rate (using Eq. 10) as a function of the number of layers, n, using the values obtained from the single layer data and assuming the minor loss coefficient K is equal to 0.4, the minor loss coefficient associated with a sudden flow contraction [9]. The density of the air, ρ, was taken to be 1.2 kg/m^3.

Initially, addition of more layers produces a nearly linear increase in the total volume flow rate. However, the pressure drop through the inlet port starts to become more significant and the volume flow rate increases more slowly. In the limit of many pumps acting in parallel, the losses in the inlet port begin to dominate and the contributions of the internal resistances in each of the pumps can be neglected. By taking the limit of Eq. 10, it can be seen that the volume flow rate through a stack approaches a limiting value as the number of layers are increased to infinity, namely:

$$\dot{V}_{max} = \sqrt{\frac{2A_2^2 \Delta P_{max}}{\rho(K+1)}} \quad (11)$$

This represents the volume flow at which the pressure sources acting in parallel balance the inlet resistance pressure drop. For the curve shown in Fig. 9, the volume flow rate reaches about 90 percent of its maximum value at about 20

layers. The addition of a layer beyond the 17th results in an incremental increase in the total volume flow rate of 1 percent or less. However, this flow circuit model does not address the thermal resistance of the device. From a heat sink design perspective, Fig. 9 gives an incomplete picture of the problem, as additional layers may prove thermally advantageous. The thermal performance of this type of heat sink is discussed by Allison [7].

To validate the flow circuit model, several tests were performed on a multilayer device. Hot wire anemometry verified the assertion that the layers have equal flows and interlayer flow resistances are negligible. Additionally, the volume flow for various numbers of layers was measured with a bag inflation test. These tests are discussed in further detail below.
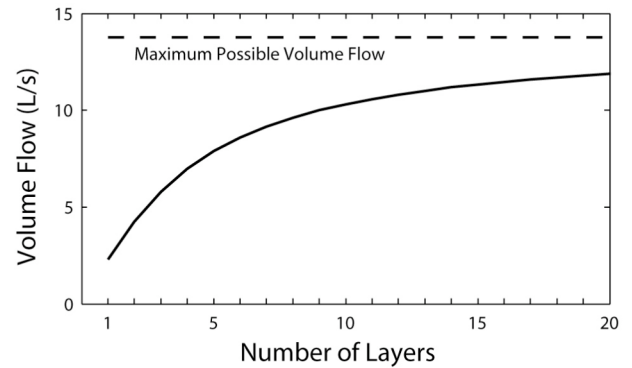

Figure 9. Total volume flow in an *n*-layer blower as a function of *n*. The curve was obtained for various *n* with *K* equal to 0.4. The maximum possible volume flow was calculated using Eq. (11).

MULTILAYER CHARACTERIZATION

A 15-layer blower was assembled and integrated with a permanent magnet motor to test the flow circuit model. The heat pipe of the overall device design was not integrated with the blower for this test. Instead, solid stainless steel plates were substituted for the condensers and the evaporator. The stainless steel plates substituted for the condensers are 101.6 mm x 101.6 mm x 2.3 mm, with a 40 mm diameter eye. The evaporator substitute is a 10 mm stainless steel plate with a close fit hole for the lower bearing. The assembly was formed by sliding all of the plates onto evenly spaced ledges in a stainless steel jig and sliding 9.5 mm diameter stainless steel rods through the holes in the four corners of the stator plates. The jig ensured parallel stators and a 2.8 mm gap space between each pair of plates. Rings of Ag-Cu-Sn braze filler metal (BAg-18) were placed around each rod-plate joint and the assembly was brazed in a vacuum furnace at 780ºC.

After brazing, the multilayer stator assembly was removed from the jig and the upper bearing housing was placed above the top stator. Aluminum impellers identical to those used for the single layer tests were slid in between each pair of stators and centered in the gaps with precision shims. A 6.4 mm

diameter stainless steel shaft was threaded through the upper bearing, the impellers, and the lower bearing and fixed in place with epoxy (DP-460NS, 3M). After the epoxy cured, the motor rotor and stator were bolted to the upper bearing housing. The full assembly is shown in Fig. 10. In the side view, it can be seen that the impellers were staggered in an attempt to reduce drag between the air flow and the impellers in the eye of the assembly. The top view shows the extent to which the motor rotor and bearing housing obstruct the inlet air. In addition, it can be seen that the inner diameter of the motor rotor is larger than the diameter of the eye in the stainless steel plates.

Two preliminary tests of the multilayer air flow were made. In the first test a hot wire anemometer was used to compare the air flow through each layer. In the second test the time required for the blower to inflate a bag was measured to get an estimate of the total air flow through the assembly.

cooling velocity as a function of distance from the bottom of the multilayer blower is shown in Fig. 11. The term "effective cooling velocity" is used to indicate that this measurement does not resolve the direction of the air flow. It can be seen in the figure that the flow is low in the first 10 mm of travel, where the anemometer is adjacent to the lower bearing housing. Across the majority of the impeller layers the flow velocity is 3 m/s. At 80 mm from the bottom of the lower bearing housing there is a peak, with the flow reaching 5 m/s and then falling to a low velocity as the anemometer passes the upper bearing housing. The hot wire anemometer measurement indicates that flow is evenly distributed between the layers except for the top layer. A peak in the flow occurs at the exit of the top layer because the diameter of the eye in the stator plates is smaller than the inside diameter of the motor rotor. The air that passes through the inside diameter of the motor but hits the top stator is forced to turn and exit through the top layer.
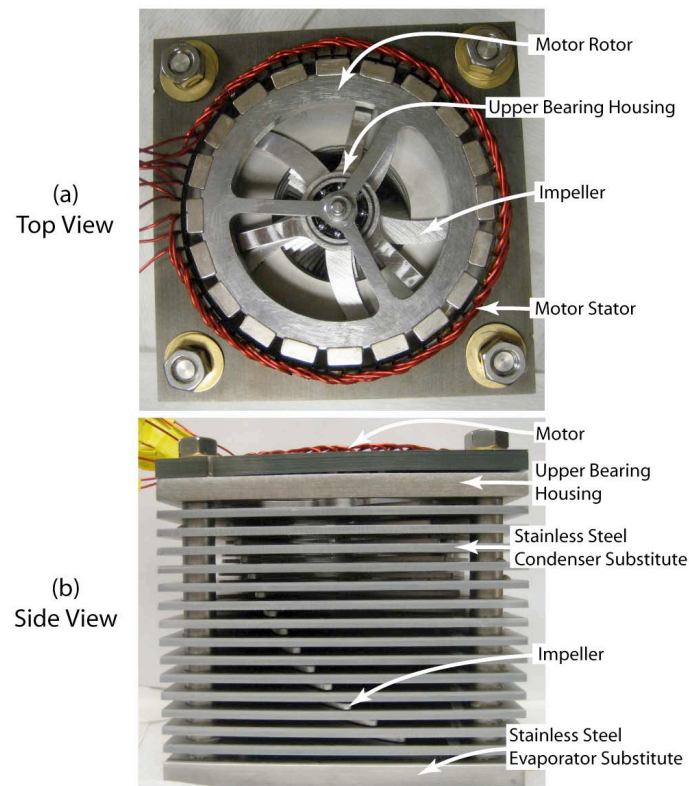

Figure 10. (a) Multilayer blower assembly. (b) Side view. The assembly is 101.6 mm (4 inches) on each side.

For the hot wire anemometer test, the anemometer (#1210-60, TSI Inc.) was placed 2 mm from the side of the multilayer blower, oriented with the wire parallel to the stator gap. The flow was profiled from the lower bearing housing to the upper bearing housing at a horizontal position halfway between the vertical rods. The anemometer was moved vertically at 1 mm/s and the anemometer voltage was recorded at a sampling rate of 100 Hz. A plot of the measured effective
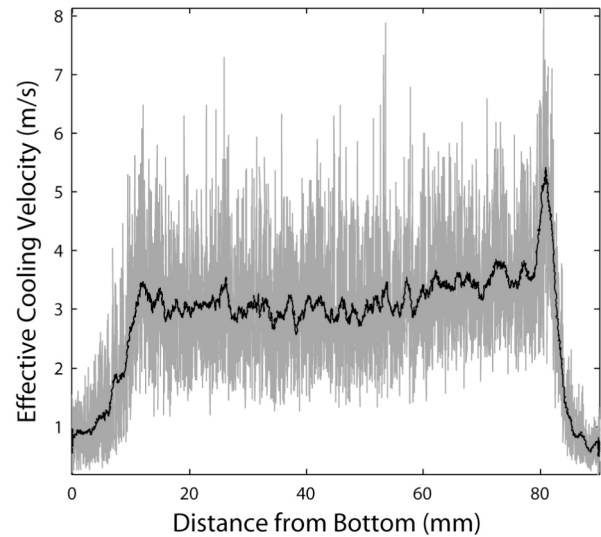

Figure 11. Effective cooling velocity as a function of position with the multilayer blower spinning at 4400 rpm. Position is measured from the bottom of the lower bearing housing to the top of the upper bearing housing. The original data is shown in gray, and the low-pass filtered data is shown in black.

For the bag inflation test, two 125 liter plastic trash bags were taped together and a 101.6 mm x 101.6 mm square was cut out. The multilayer blower was placed in the bag and the square opening was taped around the top perimeter of the motor stator so that air could only enter or leave the bag through the motor rotor. The motor was spun at 4400 rpm. When the bag was inflated it formed a cylinder on either side of the multilayer blower. The volume of the inflated bag was calculated after measuring the circumference and length of these cylinders. The bag was only inflated to about 75% of its maximum volume and a string wrapped around the perimeter was used to ensure that the bag was inflated to the same circumference in each

6   Copyright © 2010 by ASME

repetition of the test. After each repetition, the air was slowly pushed out of the bag and the bag was laid out flat next to the multilayer blower for the next repetition. The bag inflation rate was measured ten times. For the 15-layer blower, the average measured flow rate was 10.3 L/s with a standard deviation of 0.6 L/s.

The bag test was repeated with some layers of the multilayer blower blocked by tape in order to simulate blowers with different numbers of layers. As discussed above, more air flows through the top layer of the blower due to the larger inlet associated with this layer. Since the effect of this geometrical dissimilarity in the top layer was not included in the flow circuit model, the top layer was blocked in order to test the multilayer predictions with greater fidelity. The air flow rate was measured for a 5-layer, 8-layer and 14-layer blower by taping off additional layers starting from the bottom of the blower. The measured total air flow rates were 4.9, 5.4 and 7.3 L/s, respectively.

DISCUSSION AND CONCLUSION

The results of the multilayer bag tests are plotted in Fig. 12, along with a curve generated using the flow circuit model and the single layer pump curve. Additionally, a dashed line is plotted indicating the total flow rate predicted by simply multiplying the flow measured in a single layer blower by the number of layers. The flow circuit model gives a good approximation of the flow in the multilayer blowers, which is much lower than if the single blower flow is scaled linearly with n. The volume flow levels off as more layers are added due to the relative scaling of the inlet flow resistance and the flow resistance associated with each impeller layer. As more layers are added, the inlet resistance begins to dominate the flow circuit, and the impellers must pump against an increasingly large inlet to outlet pressure gradient. This results in a drop in performance, as shown in Fig. 12.

The value of the minor loss coefficient associated with the curve predicted by the flow circuit model and shown in Fig. 12 is 5.3. This value was chosen so that the curve passed through the 5-layer data point, which had the lowest uncertainty of the bag inflation test runs. While this value is larger than 0.4, it represents a flow condition much less ideal than a simple flow contraction. In the multilayer blower, the motor rotor presents several obstructions to the flow which result in additional minor loss terms. These obstructions can be seen in Fig. 10a. Furthermore, since some of the obstructions are stationary while others rotate, turbulent and unsteady flow patterns develop in the inlet which increase the loss terms. In future work, the flow circuit model will be refined to separate these losses.

The error bars associated with the bag test points in Fig. 12 are based on the estimated uncertainties in the bag volume (± 10 L) and measurement time. It takes 7-8 s for the motor to reach full speed, and the bag inflates a small amount while the motor spins up (less than about 10%). The error bars in Fig. 12 include uncertainties associated with estimating the total

volume of the bag, the amount of air in the bag at the start of the test, and the time at which the bag was deemed full. The uncertainty in the volume flow, which occurred due to propagation of these two measurement uncertainties, was assumed to be symmetric. Finally, the higher volume flow measured in the 15-layer test may be attributed to the larger flow rate through the top layer that was observed in the anemometer test plotted in Fig. 11. The top layer was blocked in the 5-, 8-, and 14-layer tests.

The bag test is not an ideal method of measuring the flow rate because it involves substantial start up transients and the air filled volume cannot be measured with great accuracy. In future work, a careful measurement of the total flow rate for the multilayer blower will be made using hot film anemometry upstream of the air inlet in a manner analogous to the single layer measurements described above.
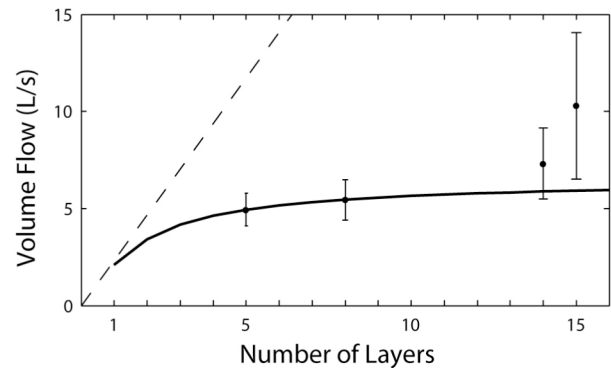

Figure 12. Volume flow versus number of layers. The points are the measured volume flows from the bag inflation tests. The dashed line represents a linearly increasing volume flow with additional layers, while the lower line is the prediction of the flow circuit model.

Blowers are often characterized alongside a system. The pump curve intersects the system resistance curve at the installed operating point. However, in this case, *in situ* characterization of the multilayer system was impractical. The flow circuit model bridges the gap between the much simpler single layer experiments and the desired information about multilayer performance.

To summarize, an experimental apparatus was constructed to characterize a single impeller and determine its pump curve. A simple flow circuit model consisting of a nonlinear resistor and a voltage source with an internal resistance was proposed to predict the hydrodynamic performance of a multilayer device based on these single layer experimental results. Hot wire anemometer tests on a 15-layer prototype device verified the assumption that the interlayer resistances in the flow circuit model are negligible. Finally, bag inflation tests at several operating points demonstrated that the flow circuit model satisfactorily predicts the performance of a device comprised of a multitude of single blowers acting in parallel and sharing a common restrictive inlet.

Copyright © 2010 by ASME

ACKNOWLEDGMENTS

NOMENCLATURE

Roman

Name	Meaning	Units
A_2	Area at point 2	m^2
I	Current	A
K	Minor loss coefficient of inlet	-
n	Number of layers	-
P_1	Pressure at point 1	Pa
P_2	Pressure at point 2	Pa
R_{elec}	Electrical resistance	Ω
R_{inlet}	Inlet flow resistance	Pa·s/m³
R_{int}	Internal flow resistance of pump	Pa·s/m³
R_{total}	Total flow resistance	Pa·s/m³
v_1	Velocity at point 1	m/s
v_2	Velocity at point 2	m/s
$\dot{V}$	Volume flow rate	m³/s
$\dot{V}_{layer}$	Volume flow rate per layer	m³/s
$\dot{V}_{max}$	Maximum volume flow rate	m³/s

Greek

Name	Meaning	Units
ρ	Density	kg/m³
ΔP_{max}	Maximum pressure rise of blower	Pa
ΔV	Voltage difference	V

REFERENCES

[1] Sathe, S., and Sammakia, B., 1998, "A Review of Recent Developments in Some Practical Aspects of Air-Cooled Electronic Packages," Journal of Heat Transfer, **120** (4), pp. 830-839.

[2] Xu, G., Guenin, B., and Vogel, M., 2004, "Extension of Air Cooling For High Power Processors," 9th Intersociety Conference on Thermal and Thermomechanical Phenomena in Electronic Systems (ITHERM), **1**, pp. 186-193.

[3] Khan, W.A., Culham, J.R., and Yovanovich, M.M., 2006, "The Role of Fin Geometry in Heat Sink Performance," Journal of Electronic Packaging, **128** (4), pp. 324-330.

[4] Dewan, A., Patro, P., Khan, I., and Mahanta, P., 2010, "The Effect of Fin Spacing and Material on the Performance of a Heat Sink with Circular Pin Fins," Proceedings of the Institution of Mechanical Engineers Part A - Journal of Power and Energy, **224** (A1), pp. 35-46.

[5] Walsh, E., Walsh, P., Grimes, R., and Egan, V., 2008, "Thermal Management of Low Profile Electronic Equipment Using Radial Fans and Heat Sinks," Journal of Heat Transfer, **130** (12), 125001.

[6] Stafford, J., Walsh, E., Egan, V., Walsh, P., Muzychka, Y.S., 2010, "A Novel Approach to Low Profile Heat Sink Design," Journal of Heat Transfer, **132** (9), 091401.

[7] Allison, J.M., 2010, "Air Flow in a High Aspect Ratio Heat Sink," M.S. Thesis, Massachusetts Institute of Technology, Cambridge, MA.

[8] Chirlian, P.M., 1969, Basic Network Theory, McGraw Hill, New York, USA, p. 115.

[9] Fay, J.A., 1994, Introduction to Fluid Mechanics, MIT Press, Cambridge, USA, Chap. 9.